Nuclear Physics A389 (1982) 120–140

INTRINSIC FRAGMENT SPINS GENERATED IN THE REACTIONS OF ^{20}Ne WITH ^{197}Au AND ^{238}U AT 12.6 MeV/NUCLEON *

D. J. MORRISSEY †, G. J. WOZNIAK, L. G. SOBOTKA, A. J. PACHECO ††, R.J. McDONALD, C. C. HSU ‡ and L. G. MORETTO

Nuclear Science Division, Lawrence Berkeley Laboratory, University of California, Berkeley, California 94720

Received 19 March 1982

Abstract: The average magnitude and alignment of the intrinsic spin of the heavy partner from the reaction of 252 MeV ^{20}Ne with ^{197}Au and ^{238}U were determined as a function of Q-value. These spin values were extracted from sequential fission angular distributions obtained in coincidence with projectile-like products. For all Q-values a large out-of-plane anisotropy was observed, while for large negative Q-values an in-plane anisotropy was observed. A very large entrance-channel mass-asymmetry was chosen to provide a stringent test of equilibrium statistical model predictions for the spin alignment. The importance of determining the direction of the line-of-centers of the dinuclear system at scission is discussed. Large values of P_{zz} were deduced for all Q-values. P_{xy} was observed to be positive in the quasielastic region and negative in the deep-inelastic region. The extracted alignment data are compared to equilibrium statistical model calculations.

E NUCLEAR REACTIONS Fission ^{238}U, ^{197}Au(^{20}Ne,F), $E = 252$ MeV; measured σ (fragment E), (fragment)(fragment)-ion, $\sigma(E_1, \phi_1, E_2, \phi_2)$, $\sigma(E_1, \phi_2, E_2, \theta_2)$; deduced fragment spin, alignment versus (Q). In-plane, out-of-plane measurements. Equilibrium statistical model.

1. Introduction

The measurement of particle and γ-ray angular distributions [1-4]) associated with deep-inelastic collisions (DIC) allows one to study the process of angular momentum transfer through the determination of the magnitude and alignment of the fragment spins. Large intrinsic spins can be introduced in the reaction products through the dissipation of entrance-channel orbital angular momentum. From mechanical considerations and from the rigid rotation limit, the fragments' spins are expected to be aligned perpendicular to the reaction plane. Misalignment of the fragments' spins occurs when in-plane components of angular momentum are present. These com-

* This work was supported by the Director, Office of Energy Research, Division of High Energy and Nuclear Physics and Nuclear Sciences of the Basic Energy Sciences Program of the US Department of Energy under Contract DE-AC03-76SF00098.

† Permanent address: Dept. of Chemistry and National Superconducting Cyclotron Lab., Michigan State University, East Lansing, Michigan, 48824.

†† Permanent address: Comision Nacional de Energia Atomica, Buenos Aires, Argentina.

‡ Permanent address: Institute of Atomic Energy, Beijing, China.

ponents can be generated either directly by some feature of the reaction mechanism, or by nonequilibrium or equilibrium statistical fluctuations in the angular-momentum-bearing modes of the dinuclear system.

Experimental techniques used to obtain the magnitude and alignment of the transferred spin include α-particle[5-7]), γ-ray[8-12]) and sequential fission fragment[13-16]) angular distribution measurements. The out-of-plane angular distributions of γ-rays and sequential fission fragments are primarily sensitive to the average random spin component. From such studies the Q-value dependence of the average misalignment has been determined[9-15]).

The angular distributions of γ-rays and α-particles are rather insensitive to differences in the in-plane projections of the random spin component[4, 7]). In contrast, the angular distributions of sequential fission fragments are quite sensitive to such differences in that they can produce a substantial in-plane anisotropy. In-plane measurements of sequential fission angular distributions[13-16]) have given conflicting results as to the existence of an in-plane anisotropy. An in-plane anisotropy has been observed[13, 15]) at low and moderate Q-values which diminished at high Q-values. However, no ansisotropy was found for a similar system[14]).

At present two theoretical explanations for the alignment have been put forth, (a) dynamical, based either on the excitation of vibrational modes[3]) or on the amount and

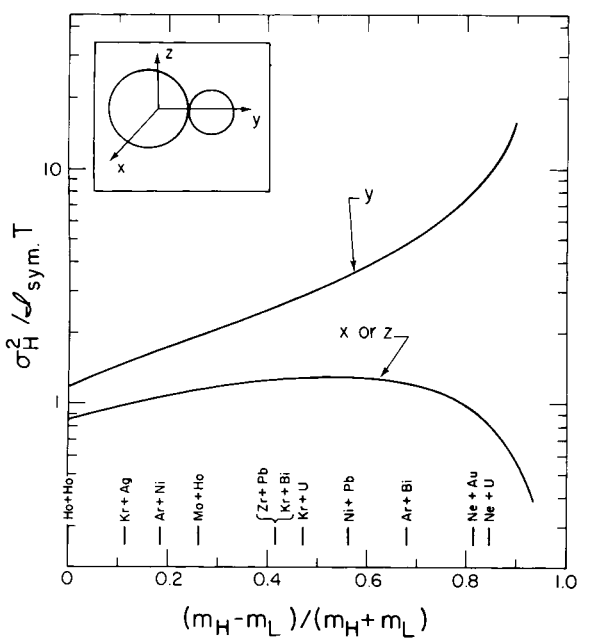

Fig. 1. The variances of the normal modes of a dinuclear complex are shown as a function of mass asymmetry of the complex. The variances are shown in dimensionless units after division by $\mathcal{I}_{sym}T$, the moment of inertia of a mass-symmetric spherical fragment times the temperature. The mass asymmetries of several reaction systems from recent determinations of the spin and/or its alignment are also shown[5,7,11-16]).

direction of the spin carried by transferred nucleons [17, 18]), and (b) equilibrium statistical based on the excitation of macroscopic normal modes of the dinuclear system [19, 20]). For the symmetric system ^{165}Ho + ^{165}Ho, the out-of-plane angular distributions of continuum γ-rays have been interpreted [11]) as evidence for the statistical equilibration of the angular-momentum-bearing modes of the dinuclear system.

In the equilibrium statistical model, the aligned spins arising from the rigid rotation of the dinuclear system couple to angular momentum components associated with the thermally excited normal modes. For a model of two touching spheres, these normal modes are called bending, twisting, wriggling and tilting [19]). The statistical widths (σ_x, σ_y and σ_z) of the angular momentum components in the usual cartesian coordinates are shown in fig. 1 as a function of mass asymmetry [20]). The contributions from the individual modes to the overall widths associated with each cartesian coordinate are given by

$$\sigma_y^2 = \sigma_{\text{tilting}}^2 + \sigma_{\text{twisting}}^2, \tag{1a}$$

$$\sigma_x^2 = \sigma_z^2 = \sigma_{\text{bending}}^2 + \sigma_{\text{wriggling}}^2. \tag{1b}$$

When the reaction partners have equal masses, the thermal widths are nearly equal [19]). At large mass asymmetry, σ_y becomes much larger than σ_x or σ_z (see fig. 1) because the statistical excitation of all of the modes except tilting is strongly suppressed [20]). In particular, a large difference in the moments of inertia associated with the two partners increases the amount of energy necessary to excite any mode in which the small fragment is forced to rotate and/or a large fraction of the angular momentum goes into orbital motion (bending, twisting and wriggling).

The tilting mode corresponds to a tilting of the disintegration axis out of the plane perpendicular to the total angular momentum. This mode is favored at large asymmetries because the rotational energies about the symmetry axis and about an axis perpendicular to it tend to become equal as the mass asymmetry goes to 1. Thus for any given temperature the mean tilting of the decay axis increases with mass asymmetry, the out-of-plane distribution broadens and the in-plane distribution becomes anisotropic. In addition, this model predicts that the maximum in the in-plane angular distribution should occur perpendicular to the line-of-centers of the dinuclear complex.

Consequently, for near symmetric systems, the statistical model [20]) predicts a very small in-plane sequential fission anisotropy ($\sim$ 1.1/1) while, for very asymmetric systems such as ^{20}Ne + ^{197}Au and ^{20}Ne + ^{238}U, this model predicts a strong in-plane anisotropy (2/1). Of course, the in-plane angular distributions of sequential fission fragments also depends on the value of K_0 (the width of the projection of the total spin on the separation axis) of the fissioning nucleus [2]) which tends to moderate the effect of differences in σ_x and σ_y on the in-plane angular distribution. (The much larger relative value of K_0 as compared with σ is responsible for the insensitivity of sequential α-decay to differences in σ_x and σ_y.)

In this paper we report measurements of sequential fission angular distributions from the reaction of 252 MeV ^{20}Ne with ^{197}Au and ^{238}U. These systems are extremely mass-asymmetric and should severely test the predictions of the equilibrium statistical model. At the same time the results of this study should shed light on the present discrepancy between previous sequential fission studies. In sect. 2 we present the experimental details of the measurements and a description of the data analysis. Sect. 3 contains the angular distribution results and a discussion of the fitting of the angular distributions. The statistical model calculations are discussed in sect. 4 and are compared to the fitted results in sect. 5. The paper is concluded in sect. 6. A brief report of this work has appeared previously [21]).

2. Experimental

A beam of 252 MeV ^{20}Ne was obtained from the 88″ cyclotron at the Lawrence Berkeley Laboratory. This beam irradiated either a metallic 915 μg/cm^2 ^{197}Au foil or a 922 μg/cm^2 UF_4 deposit on a 0.5 mg/cm^2 aluminium foil. These thicknesses were determined by weight. The target was rotated about the center of the scattering chamber both in-plane and out-of-plane to minimize corrections to the energy of the fission fragments and projectile-like products. For the ^{238}U target with the Al backing, these corrections were minimized by orienting the UF_4 deposit towards the fission fragment detector array (see below). Projectile-like fragments (PLF) were detected in a solid-state telescope (ΔE = 11 μm, E = 300 μm, dΩ = 3.0 msr) that was fixed at 30° to the beam. (For the reactions of 252 MeV ^{20}Ne + ^{197}Au and ^{238}U, the classical grazing angles in the laboratory are 26° and 30°, respectively.) The resolution of the Z-telescope was sufficient to completely separate atomic numbers between 2 and 15; however, it was insufficient to resolve the individual atomic numbers of the fission fragments.

Fission fragments (FF) were observed on the opposite side of the beam from the PLF in an array of 10 silicon surface-barrier detectors (300 μm). These detectors were held in a rigid inverted T-shaped mount suspended from the top of a hemispherical scattering chamber lid identical to the one described in ref. [7]). Both arms of the "T" were arched so that the fission detectors would remain at the same distance from the target when the laboratory angle of the entire assembly was changed. The positioning of the detectors was found to be reproducible to better than 0.5°. The solid angles subtended by the detectors were calibrated with sources (^{241}Am, ^{212}Pb and ^{252}Cf) placed in the center of the scattering chamber. All of the FF detector solid angles were determined to be 9.0 msr to within 5% and were independent of the array's position. The 10 detectors were placed on the two arms of the "T" mount with 6 (or 5) in-plane and 4 (or 5) out-of-plane with respect to the plane formed by the beam direction and the PLF telescope.

A schematic diagram of the electronics used during the measurement is shown in fig. 2. Two classes of events opened the master gate and were subsequently written onto magnetic tape; (a) scaled down Z-telescope events which were used for run-to-run

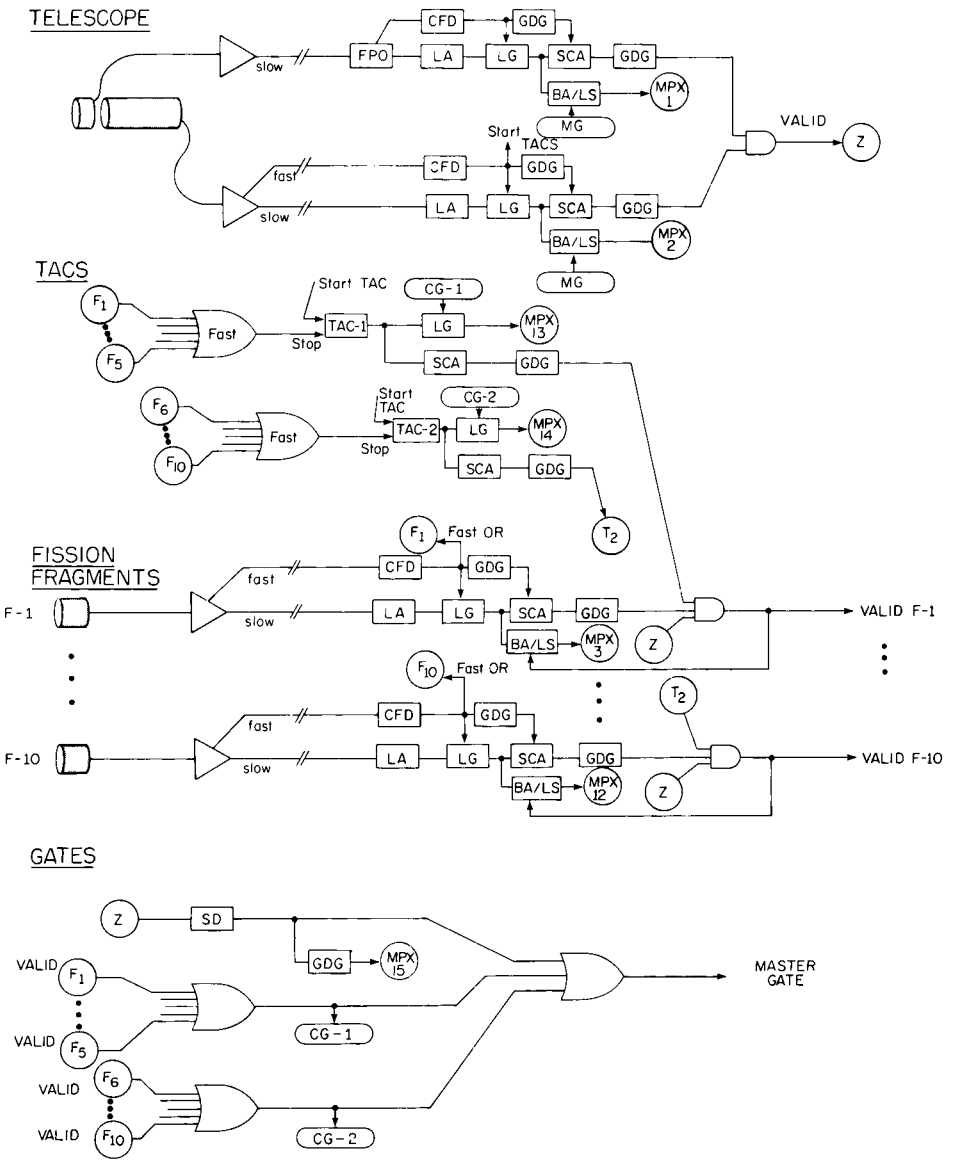

Fig. 2. A schematic diagram of the NIM electronics is shown where: BA/LS – biased amp and linear stretcher, CFD – constant fraction discriminator, CG – coincidence gate, FPO fast pick-off, GDG – gate and delay generator, LA – linear amp, LG – linear gate, MG – master gate, MPX – multiplexer input, SCA – single-channel analyser, SD – 2^N scale down.

normalization, fission probability calculations, and monitoring of the telescope resolution, and (b) valid coincidence events in which a valid Z, valid fission energy and TAC were required (see fig. 2). In fig. 3 a two-dimensional map of the fission detector's energy versus the difference in time of flight between the Z-telescope and the fission

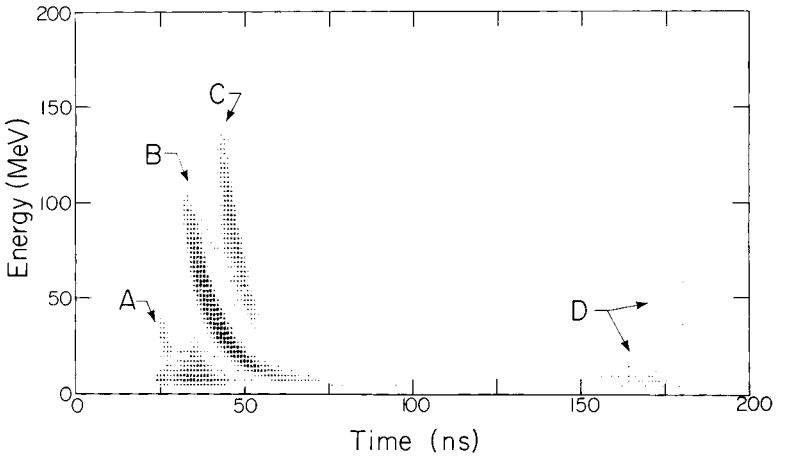

Fig. 3. An intensity plot of the coincidence data as a function of "fission fragment" energy versus time of flight. See text for discussion of groupings.

detector is shown. The various groups of events in fig. 3 were identified as arising from coincidences between (A) PLF and α-particles, (B) a pair of compound nucleus fission fragments, (C) PLF-sequential fission fragment, and (D) random coincidences with the next beam burst. The sequential fission events of interest, group C, were selected by a two-dimensional gate for further processing.

The gated coincidence data were transformed into the calculated rest frame of the recoil nucleus event by event. The above transformation relies on some straightforward trigonometric relations among the velocity vectors after the assumption of two-body

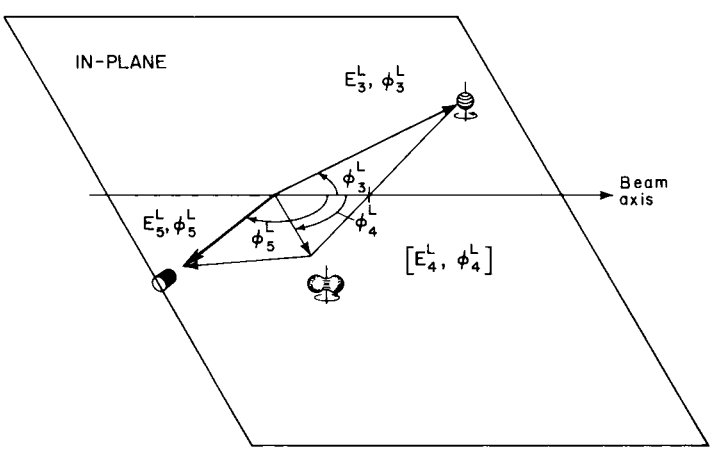

Fig. 4. The general relationships of the velocity vectors for in-plane emission are shown. The measured quantities are $E_3^L, \phi_3^L, E_5^L, \phi_5^L$; which are the lab energy and angle of the PLF and the lab energy and angle of the FF, respectively.

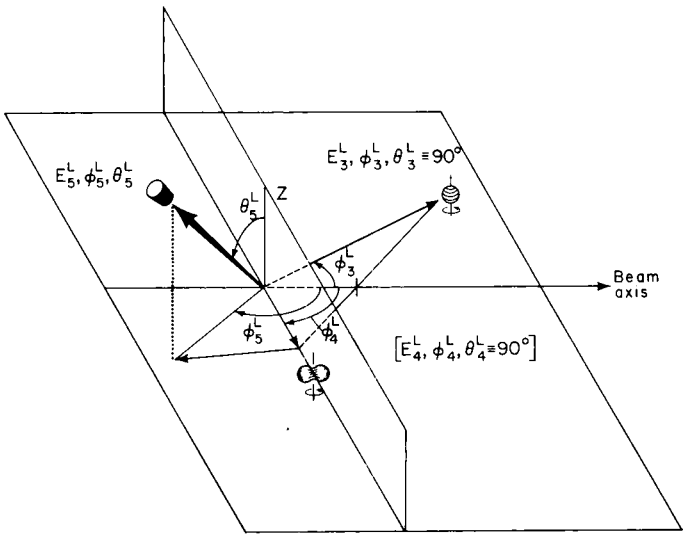

Fig. 5. Similar to fig. 4, however the fission fragment is emitted out-of-plane with respect to the PLF and the beam direction.

kinematics for the DI event. The general relationships among these vectors are shown in fig. 4 for coplanar emission and in fig. 5 for out-of-plane emission. Spherical polar coordinates are used with ϕ the in-plane angle and θ the angle from the normal to the plane.

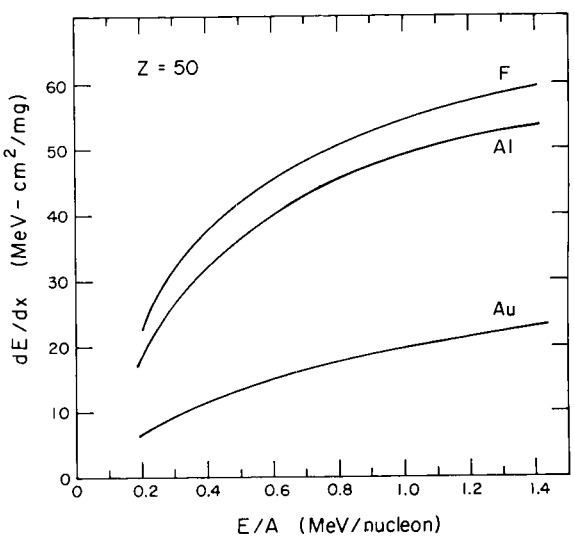

Fig. 6. Energy-loss curves are shown for a representative fission fragment traveling through fluorine, aluminum or gold [23]).

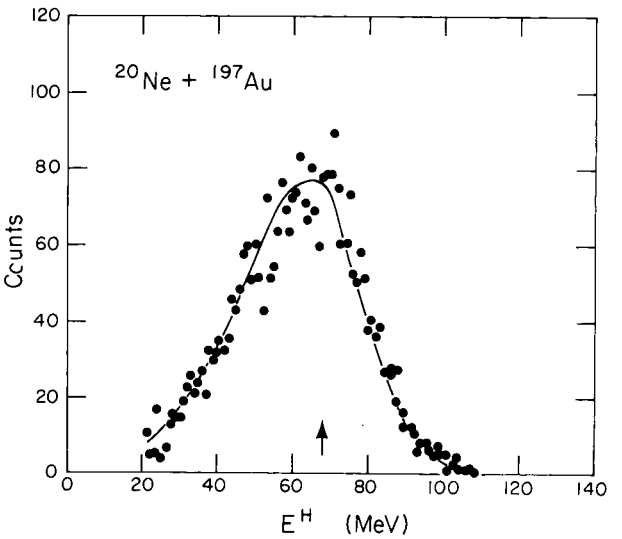

Fig. 7. The measured energy spectrum of sequential-fission fragments in the rest frame of the gold nucleus is shown. The arrow marks the single-fragment energy expected from the Viola systematics[24]). The curve drawn through the data is to guide the eye.

The observed lab energy of the PLF was corrected for pulse-height defect[22]) and energy loss in the target and any backing material[23]). These corrections for the PLF were generally small. However, the rate of energy loss (dE/dx) for the FF traveling through the target material was substantial and could be nonlinear for a slow-moving FF. This can be seen in the plot of dE/dx for typical FF energies shown in fig. 6. The measured FF energies were first corrected for pulse-height defect[22]) and then the energy-loss function was calculated in 10 steps (see fig. 6) back to the middle of the target material (Au or UF_4). In the recoil rest frame the corrected FF energy spectra were approximately gaussian shaped and peaked at energies in close agreement with Viola's predictions[24]). For example, the sequential fission fragment energy spectrum obtained with the gold target is shown in fig. 7. If the corrections due to energy loss are not done in the stepwise fashion described above, then the energy distributions broaden and peak at a lower energy.

3. Results

From the present study, angular distributions of the sequential fission-fragments are obtained in the rest frame of the recoiling target nucleus. In general, these distributions do not directly reflect the spin components of the exit channel, because they are biased by the probability that the recoil nucleus will undergo fission. Since this probability (P_f) can be strongly dependent on the excitation energy E^* and the spin I of the product

nuclei, it is important to have a rough estimate of $P_f(E^*, I)$. An estimate of the fission probability can be obtained from the calculated ratio of the neutron emission and fission widths (Γ_n/Γ_f). The dependence of this ratio on the excitation energy and spin is shown in figs. 8 and 9 for gold and uranium nuclei, respectively. The contours were calculated from a standard formula [25]). For simplicity the yrast line was calculated with the rigid-body moment of inertia. The neutron separation energy, S_n, was taken from the liquid-drop model, and the fission barrier, B_f, was taken from the rotating hquid-drop model [26]). Figs. 8 and 9 clearly indicate that requiring the target-like

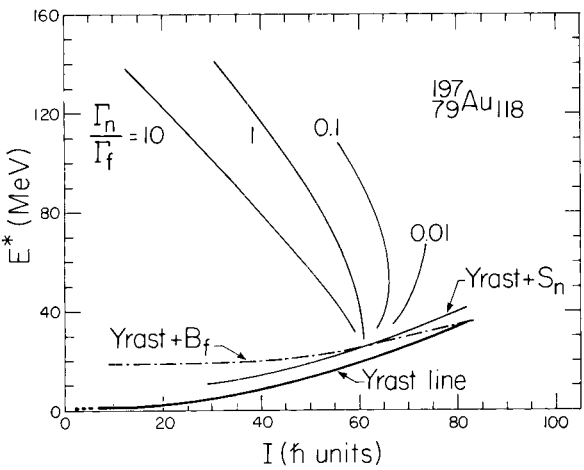

Fig. 8. Calculated contours of the ratio of the neutron emission width to the fission width, Γ_n/Γ_f, for ^{197}Au are shown as a function of excitation energy, E^*, and fragment spin, I (see text for details).

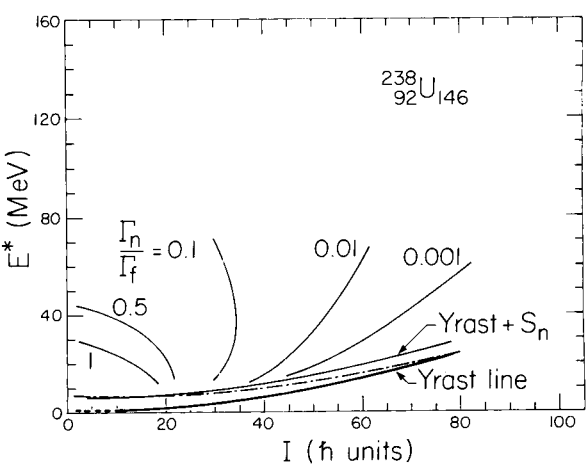

Fig. 9. Similar to fig. 8, except for ^{238}U. For ^{238}U fission decay is dominant everywhere in the E^*–I plane except at the lowest spins and excitation energies.

product to undergo sequential fission introduces a very strong bias towards high-spin states for gold nuclei but essentially no bias for uranium nuclei. Thus, the inferred average spin of the Au-like fragments which undergo fission may be very different from the average of the unbiased population.

The experimental sequential fission probabilities are shown in fig. 10. The P_f for

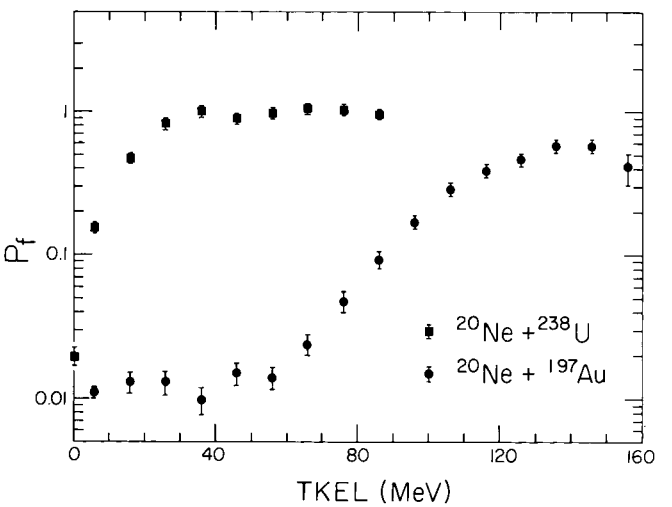

Fig. 10. The measured fission probability, P_f, is shown as a function of total kinetic energy loss, TKEL.

reactions with gold were extracted in a straightforward manner from the ratio of coincidences to PLF singles taking proper account of the fitted angular distribution of sequential-fission fragments. It was not possible to extract P_f for ^{238}U from our data for values of TKEL above 90 MeV because at larger values of TKEL the singles distribution became contaminated with reactions on the low-Z materials in the target. Because P_f saturates at a value of ~ 1 by ~ 40 MeV TKEL this limitation is unimportant. As a result of this large fission probability, substantial coincidence data was obtained over a broad TKEL range for uranium. In contrast, the maximum value of P_f for gold products is ~ 0.6 which is reached only at the largest Q-values. As a result, statistically significant angular distributions were obtained only at large values of TKEL for the gold system.

The coincidence data from the uranium target was divided into 5 TKEL bins (2 for gold) in order to investigate the in-plane and out-of-plane angular distributions. The measured FF angular distributions plotted against the out-of-plane (θ^H) and in-plane (ϕ^H) angle of the heavy recoil are shown in figs. 11 through 14. Both ϕ^H, the in-plane angle, and θ^H, the out-of-plane angle, are in the rest frame of the recoiling heavy target-like nucleus. The traditional assignment of $\phi^H = 0$ along the recoil direction (Q-value dependent) was made, with negative ϕ^H angles lying between the recoil direction and the beam axis.

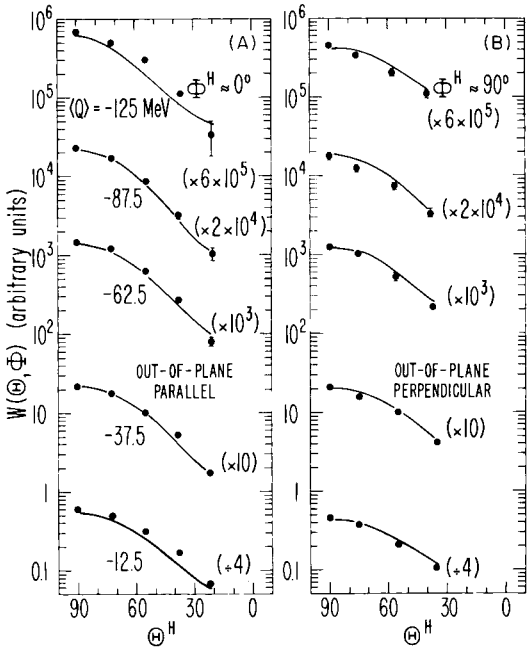

Fig. 11. The out-of-plane angular distributions of sequential FFs obtained in coincidence with PLFs of Z = 6–14 are shown for five Q-value bins for the $^{20}Ne + ^{238}U$ system. The distributions shown in part (A) were measured approximately along the laboratory recoil direction and those in (B) were obtained approximately perpendicular to the recoil direction. The solid curves represent fits described in the text.

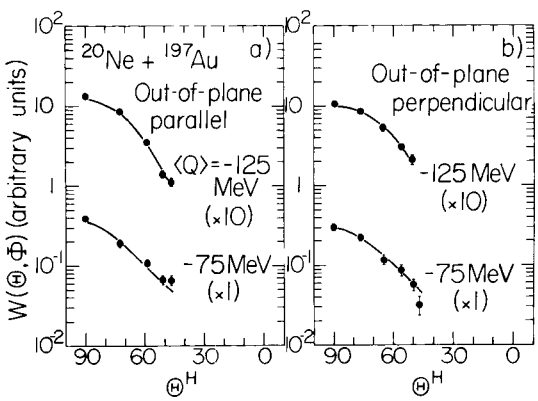

Fig. 12. The out-of-plane distributions of sequential FFs obtained in coincidence with PLFs of Z = 6–14 are shown for two Q-value bins for the $^{20}Ne + ^{197}Au$ system.

To improve statistics, all projectile-like products with Z-values between 6 and 14 were included in the Q-value gate. The two-body kinematics were calculated on an event-by-event basis assuming that the mass of the PLF was twice its atomic number. In

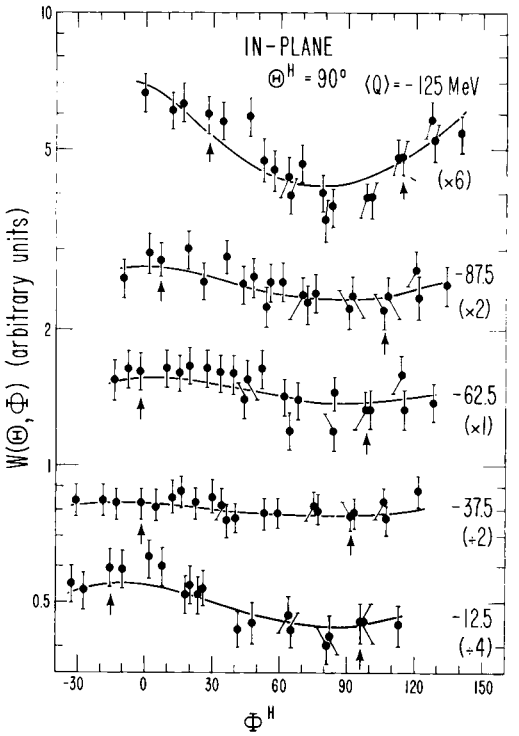

Fig. 13. In-plane angular distributions of sequential FFs from the $^{20}Ne + ^{238}U$ system are shown for the same Z- and Q-value bins as fig. 11. The arrows indicate the angles at which the out-of-plane measurements were made.

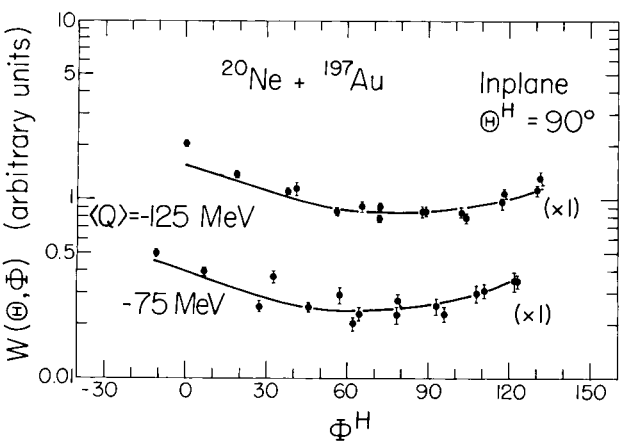

Fig. 14. In-plane angular distributions of sequential FFs for the $^{20}Ne + ^{197}Au$ system for the same Z- and Q-value bins as fig. 12.

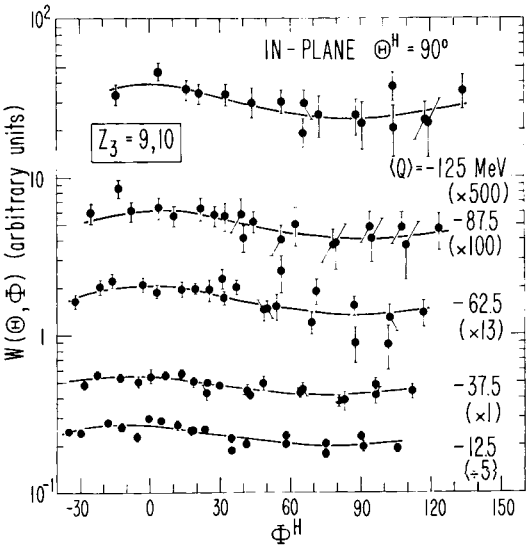

Fig. 15. The in-plane angular distributions of sequential FFs in coincidence with PLFs of $Z = 9$ or 10 from the $^{20}Ne + ^{238}U$ system are shown for the same Q-value bins as the ungated distributions shown in fig. 13 where $6 \leq Z \leq 14$.

order to verify that the calculated kinematics was not biased by evaporation over the broad range of Z-values, angular distributions were obtained for PLFs with Z-values equal to 9 or 10 for the ^{238}U system (see fig. 15). These in-plane angular distributions are very similar to the ones in fig. 13 indicating that no bias is introduced by the larger Z-value gate.

The out-of-plane angular distributions, $W(\theta^H, \phi^H)$ (measured at constant ϕ^H), fall approximately an order of magnitude over the measured θ^H range. For both systems the in-plane angular distributions show a strong anisotropy (nearly 2 to 1) at large Q-values. As the Q-value decreases, the anisotropy rapidly diminishes except for the most quasielastic bin which shows a small in-plane anisotropy. This quasielastic bin is dominated by events in which the PLF was an oxygen nucleus, suggesting that the direct transfer of an α-particle from ^{20}Ne to the target is probably the dominant reaction mechanism. Thus the anisotropy observed in this low Q-value bin is likely the result of direct processes which are not present or are much weaker in the other bins.

4. Model calculations

The magnitude and orientation of the intrinsic spin of the fissioning nucleus can be extracted from the angular distributions of the fission fragments. The angular distribution function expected from a gaussian spin distribution with its only nonzero

average component along the z-coordinate, i.e.,

$$P(I) \propto \exp - \left[\frac{I_x^2}{2\sigma_x^2} + \frac{I_y^2}{2\sigma_y^2} + \frac{(I_z - \bar{I}_z)^2}{2\sigma_z^2} \right], \tag{2}$$

has been shown to be a simple function of the parameters of the spin distribution [3,4]. The angular distribution function in the rest frame of the fissioning nucleus is:

$$W(\theta^{\mathrm{H}}, \phi^{\mathrm{H}}) \propto \frac{1}{S} \exp - \left[\frac{I_z^2 \cos^2 \theta^{\mathrm{H}}}{2S^2} \right], \tag{3}$$

where

$$S^2 = K_0^2 + (\sigma_x^2 \sin^2 \phi^{\mathrm{H}} + \sigma_y^2 \cos^2 \phi^{\mathrm{H}}) \sin^2 \theta^{\mathrm{H}} + \sigma_z^2 \cos^2 \theta^{\mathrm{H}}.$$

Our convention is that $\theta^{\mathrm{H}} = 90°$ corresponds to the in-plane measurements and that $\phi^{\mathrm{H}} = 0°$ corresponds to the separation or y-axis.

In order to use the above prescription to extract σ_x and σ_y from the FF angular distributions, the direction of the separation axis must be determined. This is not an experimental observable and must be obtained in a model-dependent way or left as a free parameter. In the limit of an elastic collision between rigid spheres, the separation axis coincides with the laboratory recoil direction as suggested in ref. [2]. In the other limit of zero exit channel angular momentum, as in spontaneous fission, the separation axis corresponds to the center of mass (c.m.) recoil direction. Deeply-inelastic heavy-ion reactions lie in between these two limits.

Previous measurements have ignored this problem and simply used the laboratory recoil direction for the separation axis [13-15]. This direction is appropriate under the strongly selective conditions present in sequential fission induced [27] by light-ions [i.e., (d, pf) or (α, α'f)]. However, in inelastic heavy-ion reactions, the two directions do *not* coincide because any decrease in the amount of orbital angular momentum between the entrance and exit channels forces the separation axis to shift away from the laboratory recoil direction towards the c.m. recoil direction (a shift towards more positive angles in the present study, see fig. 16). This shift angle χ^{H} is measured in the recoiling rest frame from the laboratory recoil direction. The shift angle was included in the fitted function by replacing ϕ^{H} by $\phi^{\mathrm{H}} + \chi^{\mathrm{H}}$ in eq. (3). The value of χ^{H} was determined by two different means, (a) as a free parameter in the chi-squared minimization, and (b) by a calculation of the orbital angular momenta contributing to each Q-value range.

The first method with the inclusion of an unconstrained shift angle into any angular distribution function is problematic because this creates a periodic minimum in the chi-squared. Rotation of $\frac{1}{2}\pi$ commutes σ_x with σ_y and rotation of π returns the original function (due to the $\cos^2$ and $\sin^2$ terms). Fits to the angular correlation data where χ^{H} was constrained to be near 0° for the quasielastic bins and near 90° for the most

inelastic bins are shown by the solid curves in figs. 11 through 15. The values of K_0^2 for uranium were calculated with the empirical function of the excitation energy, E^*, above the fission barrier, B_f, used in ref. [15]),

$$K_0^2 = 19.4(E^* - B_f)^{\frac{1}{2}}. \tag{4}$$

The K_0^2 values for gold were obtained by scaling the uranium constant by the ratio of the moments of inertia at the saddle point, $\mathcal{I}_{\text{eff}}$, from the liquid-drop model [28]). Since $K_0^2 = \mathcal{I}_{\text{eff}} T/\hbar^2$, then

$$K_0^2(\text{Au}) = \frac{\mathcal{I}_{\text{eff}}(\text{Au})}{\mathcal{I}_{\text{eff}}(\text{U})} K_0^2(\text{U}). \tag{5}$$

TABLE 1

Results of angular distribution fitting including a free rotation angle χ^H: errors are given in parentheses.

Q-value	K_0	I_z ($\hbar$)	σ_y ($\hbar$)	σ_x ($\hbar$)	σ_z ($\hbar$)	χ^H (degrees)
(a) uranium results with $6 \leqq Z_3 \leqq 14$						
− 12.5	7.3	17.7(0.5)	3.0(0.6)	6.5(0.4)	2.8(0.4)	8(7)
− 37.5	10.4	27.2(0.2)	7.7(0.2)	8.8(0.2)	1.9(0.5)	16(9)
− 62.5	12.0	31.1(0.3)	9.5(0.5)	5.8(0.7)	3.1(0.7)	90(9)
− 87.5	13.1	37.9(0.3)	13.0(0.7)	8.6(0.9)	5.3(0.5)	94(9)
−125	14.3	42.4(0.6)	20.1(0.7)	0.7(4)	9.2(1.1)	80(3)
(b) uranium results with $9 \leqq Z_3 \leqq 10$						
− 12.5	7.3	16.7(0.5)	2 (0.8)	7.1(0.4)	0.5(1)	− 9(6)
− 37.5	10.4	25.0(0.3)	3.5(0.6)	10 (0.6)	7.2(0.8)	−10(4)
− 62.5	12.0	32.2(0.5)	17 (1)	6 (1)	5 (1)	90(5)
− 87.5	13.1	45 (1)	23 (2)	8 (2)	15 (1)	81(6)
−125	14.3	37 (0.9)	22 (2)	7 (2)	0 (4)	87(7)
(c) statistical model *						
− 12.5			16.6	5.0	5.0	45
− 37.5			21.8	6.5	6.5	60
− 62.5			24.7	7.4	7.4	70
− 87.5			26.8	8.1	8.1	75
−125			28.8	8.8	8.8	80
(d) gold results with $6 \leqq Z_3 \leqq 14$						
− 75	9.8	61 (1)	25.2(0.8)	7 (2)	24 (1)	64(3)
−125	11.7	65 (1)	30.0(0.8)	0 (5)	15 (1)	79(1)
(e) statistical model *						
− 75			20.6	7.4	7.4	72
−125			23.4	8.4	8.4	80

The errors listed in this table represent only the statistical error.

* Two touching spheres.

The average energy of the fission barrier was obtained from the droplet model [29]). The numerical results of this fitting process are given in table 1. Unfortunately the numerically best choice for χ^H does not have a smooth dependence on Q-value, because of the shallowness of the angular distributions and the size of the errors in the data points at intermediate Q-values. This has been demonstrated by fitting the angular distributions with fixed shift angles (see below).

In an alternate procedure, the shift angle was estimated simply from the average change in orbital angular momentum for each Q-value. The initial orbital angular momentum, L_i, was obtained by dividing a triangular l-distribution in proportion to the cross section. The amount of exit channel angular momentum, L_f, is then written classically as:

$$L_f = L_i - \langle I_T \rangle - \langle I_P \rangle, \tag{6}$$

where $\langle I_T \rangle$ and $\langle I_P \rangle$ are the average intrinsic spins of the target-like and projectile-like fragments. The fragment spins are taken to be primarily aligned as indicated by previous results. For a rigidly rotating complex the ratio $\langle I_T \rangle / \langle I_P \rangle$ is proportional to the ratio of the moments of inertia $\mathcal{I}_T/\mathcal{I}_P$ which is 67:1 for the uranium system (45:1, for the gold system). The values of $\langle I_T \rangle$ were obtained from the out-of-plane distributions and, on the basis of the large ratios of the moments of inertia, $\langle I_P \rangle$ was ignored.

Previous studies of the reaction of ^{20}Ne with ^{197}Au indicate that at the grazing angle the scattering is predominantly occurring on the same side of the nucleus and that orbiting through zero degrees is negligible [30]). The direction of the line-of-centers for the ^{20}Ne + ^{197}Au and ^{20}Ne + ^{238}U systems was determined by tracing the projectile-like product backward along a Coulomb trajectory to the point of contact. Contact was assumed to occur at a distance given by the equilibrium configuration of a rotating

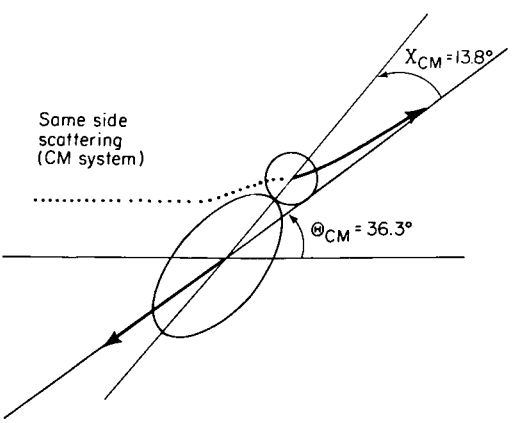

Fig. 16. The approximate shape of the ion-ion complex for the ^{20}Ne + ^{238}U reaction as estimated in a rotating liquid-drop sphere-spheroid model. The center-of-mass scattering angle is indicated as well as the shift angle relative to the c.m. separation axis.

sphere-spheroid liquid-drop model system [7]). The approximate shape of the ion-ion complex given by this schematic model for the most inelastic Q-bin is shown in fig. 16.

The resulting shift angles are 45°, 60°, 70°, 75° and 80° for the five uranium Q-value bins. For the three most negative Q-value bins these numbers are in reasonable agreement with the values returned from the fitting process for the optimum χ^H (table 1). In addition, the flatness of the angular distribution associated with the $Q = -37.5$ MeV bin causes the fitted function to be rather insensitive to χ^H for this bin. Thus, when the angular distributions were refit using the estimated values of χ^H as constants, the results for the spin distribution parameters were the same within errors, except for the -12.5 MeV bin. The exception for the Q-value of -12.5 MeV is due to an overestimation of the shift angle. Because of the unreliability of our model in this low Q-value region and the likely strong contribution from direct reaction processes, this particular discrepancy is not too discomforting.

The values of the aligned spin $\langle I_z \rangle$ and the thermal widths extracted from the fitting of the sequential fission fragment angular distributions can be utilized to determine the two alignment parameters P_{ZZ} and P_{XY} [ref. [31])]. These two parameters are defined in terms of the x-, y- and z-components of the angular momentum vector as:

$$P_{ZZ} = \tfrac{3}{2}\frac{\langle I_z^2 \rangle}{\langle I^2 \rangle} - \tfrac{1}{2} = \frac{2\langle I_z^2 \rangle - \langle I_x^2 \rangle - \langle I_y^2 \rangle}{2\langle I^2 \rangle}, \tag{7}$$

$$P_{XY} = \frac{\langle I_x^2 - I_y^2 \rangle}{2\langle I^2 \rangle}. \tag{8}$$

Taking the previous assumption of a gaussian spin distribution peaked at $I_x = 0$, $I_y = 0$ and $I_z = \langle I_z \rangle$, the alignment parameters can be rewritten in terms of fitted widths [20]) by recalling the definition

$$\langle I_x^2 \rangle = \langle I_x \rangle^2 + \sigma_x^2. \tag{9}$$

Thus, eqs. (7) and (8) become:

$$P_{ZZ} = \tfrac{3}{2}\frac{(\langle I_z \rangle^2 + \sigma_z^2)}{(\sigma_x^2 + \sigma_y^2 + \langle I_z \rangle^2 + \sigma_z^2)} - \tfrac{1}{2}, \tag{10}$$

$$P_{XY} = \frac{\sigma_x^2 - \sigma_y^2}{2(\sigma_x^2 + \sigma_y^2 + \langle I_z \rangle^2 + \sigma_z^2)}. \tag{11}$$

5. Discussion

In table 1 are shown values of I_z, σ_y, σ_x and σ_z extracted from the sequential fission fragment angular distributions. To make clearer the Q-value dependence of I_z, the extracted values of I_z are plotted versus Q-value in fig. 17 for both the $^{20}Ne + ^{238}U$ and

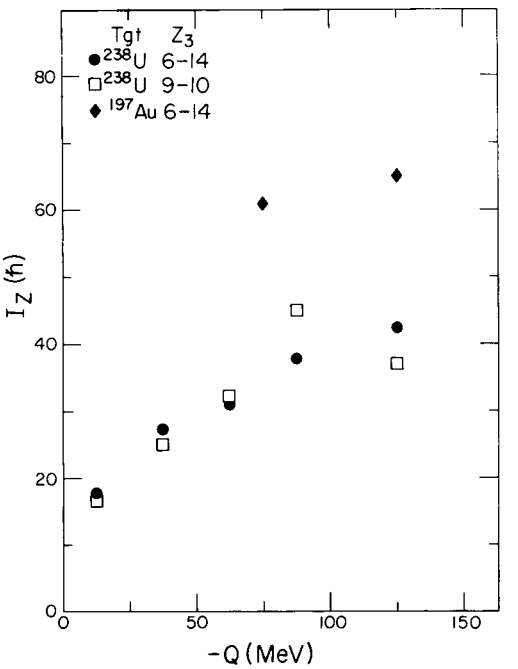

Fig. 17. The measured aligned spin (I_z) of the target-like fragment as a function of Q-value for the 252 MeV $^{20}Ne + ^{197}Au$ and ^{238}U reactions. Spins were extracted for a broad Z-bin (6–14) for both systems and an additional narrow one (Z = 9–10) for the $^{20}Ne + ^{238}U$ system. The statistical errors are of the same size or smaller than the symbols.

$^{20}Ne + ^{197}Au$ systems. For the former system, I_z increases steadily with Q-value. A similar increase of I_z with Q-value has been observed in several other reaction systems [11, 14, 15]). Because of the high fission barriers for nuclei near Au, values of I_z were obtained only for the most negative Q-values of the $^{20}Ne + ^{197}Au$ reaction. A striking difference between the two systems is the much larger values of I_z observed for the $^{20}Ne + ^{197}Au$ relative to the $^{20}Ne + ^{238}U$ system. Since the l_{max} and the rigid rotation partition for the two systems are very similar, the difference most likely reflects the strong bias towards high-spin states for the fissioning gold nuclei and the absence of such a bias for the fissioning uranium nuclei. This bias is introduced by the large fission barrier for gold nuclei (see figs. 8 and 9 and related discussion in sect. 3).

Although there is a substantial scatter in the values of the thermal widths (see table 1) extracted from the $^{20}Ne + ^{238}U$ sequential fission fragment angular distributions,

qualitatively σ_x and σ_z seem to be independent of Q-value whereas σ_y increases dramatically with Q-value. The statistical model predictions for σ_x and σ_z are in rough agreement with the data for all Q-values. However, this model substantially overpredicts σ_y except at the most negative Q-values where rough agreement is observed. Over the more limited Q-value range of the $^{20}Ne+^{197}Au$ data, the model predictions are in rough agreement with the extracted values for all three thermal widths.

The results for P_{ZZ} and P_{XY} obtained from the fitting of the FF angular distributions for the uranium system are shown in fig. 18. In contrast to the strong Q-value dependence observed in more symmetric systems [cf. e.g. refs. [11, 14, 15])], the extracted values of P_{ZZ} are approximately constant at 0.8 for the $^{20}Ne+^{238}U$ system. The in-plane alignment parameter shows a stronger dependence on Q-value. It is positive at small Q-values and then goes to negative values at larger Q-values.

The predictions of the statistical equilibrium model for two touching spheres (solid curves in fig. 18) lie substantially below both the P_{ZZ} and P_{XY} data. Although this discrepancy could be interpreted as indicating that the dinuclear system is not at equilibrium (with respect to the normal modes), a more likely explanation is that the

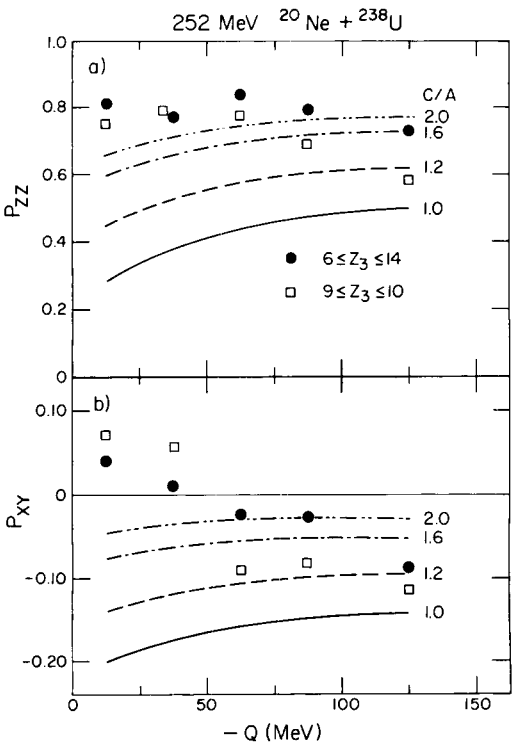

Fig. 18. The measured alignment parameters for the spin distributions obtained for the $^{20}Ne+^{238}U$ system are shown for $Z = 6$ to 14 (circles) and $Z = 9$ and 10 (squares). The solid and dashed curves represent the statistical equilibrium model calculations for different ratios of axes (C/A) of the target-like fragment (see text).

present model of two touching spheres does not allow for either deformation or interfragment separation (neck formation). Indeed, there is extensive evidence for large deformations of the nuclei at their scission configuration following a DIC [refs. [7, 32])]. A first-order estimate of the effect of deformation on the model calculations can be made by allowing the target-like fragment to deform along the line-of-centers of the dinuclear system. Model calculations of P_{ZZ} and P_{XY} are shown in fig. 18 for different ratios of axes (C/A) of the target-like fragment. Both P_{ZZ} and P_{XY} are quite sensitive to the deformation of the heavy fragment. In this calculation, σ_x and σ_z increase slowly whereas σ_y decreases rapidly with increasing C/A. Thus increasing C/A causes P_{ZZ} to increase because the random component of spin decreases while the aligned component is constant. P_{XY} approaches zero as C/A increases because σ_y becomes similar to σ_x. In this model, a ratio of axes of 1.6 to 2.0 is needed to reproduce the data in the deep-inelastic Q-value region. Such deformations of the heavy fragment are consistent with values given by the equilibrium configuration of a rotating sphere-spheroid liquid-drop model system [7]).

6. Conclusions

In this paper we have reported the fission fragment angular distributions and fission probabilities observed in coincidence with projectile-like products from the reactions of ^{20}Ne with ^{197}Au and ^{238}U at 252 MeV. A strong focusing of the fission fragments into the reaction plane is observed at all Q-values, as in previous sequential-fission studies [13-16]). In addition, sequential-fission fragments from reactions with the largest energy losses exhibited an in-plane anisotropy. At intermediate Q-values this anisotropy diminished. If the data were integrated over all Q-values, the anisotropy would be washed out because the number of quasielastic events is larger than the number of inelastic events. The importance of recognizing the direction of the body-symmetry axis as compared to the laboratory recoil direction in a deep-inelastic reaction has been pointed out. A comparison of our data with the statistical equilibrium model indicates that the target-like fragment may be substantially deformed for very inelastic collisions.

In the context of previous measurements of sequential fission, at the *largest Q-values* a qualitative pattern with mass-asymmetry is seen; the most mass-symmetric systems show a small [14, 15]) or moderate [13]) in-plane anisotropy, a more asymmetric system shows a moderate [16]) in-plane anisotropy, and the very asymmetric systems presented here show a larger in-plane anisotropy. This rough qualitative trend is in agreement with the predictions of statistical equilibrium of the normal modes of the dinuclear complex [20]). In general the technique of measuring the complete angular distributions of sequential fission fragments represents an extremely powerful tool for the study of angular momentum transfer in deeply inelastic collisions.

This work was supported by the Director, Office of Energy Research, Division of High Energy and Nuclear Physics and Nuclear Sciences of the Basic Energy Sciences Program of the US Department of Energy under Contract DE-AC03-76SF00098.

References

1) M. Lefort and C. Ngô, Riv. Nuovo Cim. **2** (1979) 1
2) B. B. Back and S. Bjørnholm, Nucl. Phys. **A302** (1978) 343
3) R. A. Broglia, G. Pollarolo, C. H. Dasso and T. Døssing, Phys. Rev. Lett. **43** (1979) 1649
4) L. G. Moretto, S. K. Blau and A. J. Pacheco, Nucl. Phys. **A364** (1981) 125
5) R. Babinet, B. Cauvin, J. Girard, J. M. Alexander, T. H. Chiang, J. Galin, B. Gatty, D. Guerreau and X. Tarrago, Z. Phys. **A295** (1980) 153
6) W. Kühn, R. Albrecht, H. Damjantschitsch, H. Ho, R. M. Ronningen, J. Slemmer, J. P. Wurm, I. Rode and F. Scheibling, Z. Phys. **A298** (1980) 95
7) L. G. Sobotka, C. C. Hsu, G. J. Wozniak, D. J. Morrissey and L. G. Moretto, Nucl. Phys. **A371** (1981) 510
8) M. N. Namboodiri, J. B. Natowitz, P. Kasiraj, R. Eggers, L. Adler, P. Gonthier, C. Cerruti and S. Simon, Phys. Rev. **C20** (1979) 982
9) K. Van Bibber, R. Ledoux, S. G. Steadman, F. Videbaek, G. Young and C. Flaum, Phys. Rev. Lett. **38** (1977) 334
10) R. J. Puigh, H. Doubre, A. Lazzarini, A. Seamster, R. Vandenbosch, M. S. Zisman and T. D. Thomas, Nucl. Phys. **A336** (1980) 279
11) R. J. McDonald, A. J. Pacheco, G. J. Wozniak, H. H. Bolotin, L. G. Moretto, C. Shück, S. Shih, R. M. Diamond and F. S. Stephens, Nucl. Phys. **A373** (1982) 54
12) A. Lazzarinni, V. Metag, A. G. Seamster, R. Vandenbosch and R. Loveman, Phys. Rev. Lett. **46** (1981) 988
13) P. Dyer, R. J. Puigh, R. Vandenbosch, T. D. Thomas, M. S. Zisman and L. Nunnelley, Nucl. Phys. **A322** (1979) 205
14) D. v. Harrach, P. Glässel, Y. Civelekoglu, R. Männer and H. J. Specht, Phys. Rev. Lett. **42** (1979) 1728
15) R. J. Puigh, P. Dyer, R. Vandenbosch, T. D. Thomas, L. Nunnelley and M. S. Zisman, Phys. Lett. **86B** (1979) 24
16) C. Le Brun, J. F. Lecolley, F. Lefebvres, M. L'Haridon, A. Osmont, J. P. Patry, J. C. Steckmeyer and R. Chechik, Phys. Rev. **C25** (1982) 3212
17) G. Wolschin, Nucl. Phys. **A316** (1979) 146
18) R. Vandenbosch, Phys. Rev. **C20** (1979) 171
19) L. G. Moretto and R. P. Schmitt, Phys. Rev. **C21** (1980) 204
20) R. P. Schmitt and A. J. Pacheco, Nucl. Phys. **A379** (1982) 313
21) D. J. Morrissey, G. J. Wozniak, L. G. Sobotka, A. J. Pacheco, C. C. Hsu, R. J. McDonald and L. G. Moretto, Z. Phys. **A305** (1982) 131
22) J. B. Moulton, J. E. Stephenson, R. P. Schmitt and G. J. Wozniak, Nucl. Instr. **157** (1978) 325
23) G. U. Rattazzi, R. P. Schmitt, G. J. Wozniak and L. G. Moretto, Lawrence Berkeley Lab Report LBL-9711 (1980) 130, unpublished
24) V. E. Viola, Jr., Nucl. Data **A1** (1966) 391
25) R. Vandenbosch and J. R. Huizenga, Nuclear fission (Academic Press, New York, 1973), eq. VII-7
26) S. Cohen, F. Plasil and W. J. Swiatecki, Ann. of Phys. **82** (1974) 557
27) See, for example, K. L. Wolf, R. Vandenbosch and W. D. Loveland, Phys. Rev. **170** (1968) 1059
28) S. Cohen and W. J. Swiatecki, Ann. of Phys. **22** (1963) 406
29) W. D. Myers, Droplet model of atomic nuclei (IFI/Plenum, NY, 1977)
30) G. J. Mathews, J. B. Moulton, G. J. Wozniak, B. Cauvin, R. P. Schmitt, J. S. Sventek and L. G. Moretto, Phys. Rev. **C25** (1982) 300
31) D. M. Brink, Phys. Lett. **40B** (1972) 37
32) K. E. Rehm, H. Essel, P. Sperr, K. Hartel, P. Kienle, H. J. Körner, R. E. Segel and W. Wagner, Nucl. Phys. **A366** (1981) 477